Available online at www.synsint.com

Synthesis and Sintering

ISSN 2564-0186 (Print), **ISSN** 2564-0194 (Online)

Research article

Reactive spark plasma sintering of ZrB_2-TiC composites: Role of nano-sized carbon black additive

Hamid Istgaldi [a], **Mehdi Mehrabian** [b], **Faramarz Kazemi** [c], **Behzad Nayebi** [c,*]

[a] *Department of mechanical Engineering, University of Mohaghegh Ardabili, Ardabil, Iran*
[b] *School of Metallurgy and Materials Engineering, Iran University of Science and Technology, 1684613114, Tehran, Iran*
[c] *Department of Materials and Metallurgical Engineering, Amirkabir University of Technology (Tehran Polytechnic), Tehran, Iran*

A B S T R A C T

ZrB_2-TiC composites with and without nano-sized carbon black as the sintering additive were densified through spark plasma sintering at 1900 °C for 7 minutes under the applied pressure of 40 MPa. The role of carbon black in densification behavior, phase arrangement, microstructural characteristics and mechanical properties of the sintered composites were then investigated. While both of the composite samples were found to be fully sintered, the thermodynamic of the reactive sintering was also studied. The results indicated that whereas the reactive sintering process leads to the complete consumption of TiC through the formation of the solid solution as the matrix in both of the composite samples, the presence of carbon black at the initial composition of the samples can result in remained carbon at the final microstructure. Besides the in-situ synthesized zirconium carbide as the major reinforcement phase, such a remained carbon can lead to significantly different mechanical behavior of the composites. Accordingly, the hardness of 21.8 and 24.3 GPa and the indentation fracture toughness of 3.3 and 4.5 MPa.$m^{0.5}$ were obtained for carbon-black free and doped samples, respectively. The densification, hardening, and toughening mechanisms in both of the composite samples were finally discussed.

K E Y W O R D S

Spark plasma sintering
Zirconium diboride
Titanium carbide
In-situ synthesis
Toughening mechanism

OPEN ACCESS

1. Introduction

Among the ultra-high temperature ceramics, zirconium diboride has been at the center of attention mainly due to its high hardness and melting point accompanied by relatively low density. The material also presents favorable thermal shock resistance as well as chemical inertness compared to most of the refractory and hard materials [1, 2]. Hence, extended research works have been dedicated to the applications of ZrB_2 as a structural material for extreme environments [3–5], such as the thermal-resistance systems of hypersonic vehicles and the leading edges of satellites and missiles. The material has also presented promising capabilities to be used in furnace refractories, the coatings of plasma welding electrodes, and recently, machining and cutting tools [5–10].

Besides its unique combination of properties, zirconium diboride encounters two main technical drawbacks. First, the very strong covalent atomic bonds which decrease the atomic diffusion rate and result in poor sintering and densification behavior, and consequently limit the industrial manufacturing of ZrB_2-based components to the expensive high-temperature and pressurized sintering techniques. Secondly, even at very high sintering temperatures and pressures (e.g., hot-pressing and/or hot-isostatic pressing), the material experiences higher grain boundary diffusion rate compared to the favorable bulk atomic diffusion rate. Therefore, the final microstructure of the sintered

* Corresponding author. *E-mail address:* behzad.nayebi@aut.ac.ir (B. Nayebi)
Received 27 February 2022; Received in revised form 10 May 2022; Accepted 10 May 2022.

https://doi.org/10.53063/synsint.2022.22107

ceramic would encounter an excessive grain growth which itself results in poor toughening behavior. In addition to the strong covalent atomic bonds, ZrO_2 and B_2O_3 oxide impurities at the surface of ZrB_2 powder particles have been revealed as the main cause of the aforementioned drawbacks [11, 12].

As a whole, the efforts to overcome the drawbacks of ZrB_2 can be categorized into two main approaches, including the fast sintering methods and using the secondary phases (composite making) and sintering additives, to reduce grain coarsening. Despite the fact that the former approaches, including microwave (MWS) and spark plasma sintering (SPS), are limited by the size and the geometry of final components, the later strategies are extensively followed by researchers and engineers as they can be used for components with different shapes and dimensions [13].

The secondary phases used in the sintering of ZrB_2 can themselves be regarded as two leading classes, consisting of reinforcements (strengthening the matrix) and sintering aids (enhancing the sinterability) [14]. Even though reinforcements are principally selected based on their mechanical and physical properties, as well as their reactivity with the matrix materials, most of sintering aids are used to remove oxide impurities and activate sintering mechanisms at interfaces.

Carbon compounds have been widely used as both the reinforcements and additives of ZrB_2-based composites [13]. Incidentally, carbides have shown great outcomes as the reinforcement and have resulted in improved mechanical properties and oxidation resistance, while many of the carbonaceous materials such as graphite, graphene, and carbon black are known as effective sintering aids owing to their reactivity with the surface oxide impurities of ZrB_2 particles [13–16].

Among carbides, silicon carbide (SiC) has been extensively applied to reinforce zirconium diboride ceramics. Admittedly, titanium carbide (TiC) is also known as an effective reinforcement, which not only inhibits the destructive grain coarsening and consequent fracture toughness drop of ZrB_2 during sintering, but also improves the densification behavior and oxidation resistance of material through the formation of ZrB_2-TiB_2 solid solution [14–16]. Titanium carbide, itself, is known as super hard, chemically stable, wear-resistant, and low coefficient thermal expansion (CTE) UHTC. Such a combination of properties provides the material potentially promising applications in cutting tools, jet engine components, and rocket nozzles [13, 15–18]. Hence, ZrB_2-TiC composite has been extensively attended recently and several research works are currently focused on developing this class of UHTC composites. However, the common shortcomings of UHTCs such as poor sintering and densification behaviors are still remained challenging.

Among several sintering methods which have been followed to manufacture relatively dense and tough UHTCs [19, 20], spark plasma sintering (SPS) provides improved outcomes, particularly at lower sintering temperatures and very short dwelling times [21, 22]. The process uses high voltage direct electrical current to form electrical discharge (spark) between the adjacent particles of the densifying powders and hence, improve the kinetic of the sintering process. The consequent high temperature plasma then activates the evaporation/densification mechanism which not only removes the surface impurities, but also provides a very fast heating rate of particles. SPS has been successfully utilized in the densification of lots of hard-to-sinter ceramic materials [23–26]. On the word of UHTCs, sintering aids have also been found as supporting materials by which, the sinterability, microstructure, and mechanical properties of the SPSed materials are improved [27, 28]. For the purpose of illustration, the fracture toughness of ZrB_2-based ceramics can be improved through activating some of the fracture toughness mechanisms such as crack deflection, crack branching, and crack bridging [29–33]. The sinterability and fracture toughness of ZrB_2-based ceramics are heightened by adding carbon nanotubes (CNTs), according to the recent reports [34, 35]. It is worthy to note that the aforementioned mechanisms also play an effective role in hardening the ZrB_2-SiC composites reinforced by short carbon fibers [36, 37]. In contrast, the fracture toughness and densification behavior of a sample are lessened by unconditionally increasing carbon fibers in the ZrB_2-SiC composites manufactured by the pressure-less sintering method [38].

While the weak interfaces and the presence of micro-cracks in ceramic matrixes may lead to crack deflection, bridging, and propagation as well as the stress adsorption at the micro-cracks (as effective toughening mechanisms), dramatically decreased hardness and strength would be observed as the side effects. Hence, using the additives which provide the mentioned toughening mechanisms without any destructive effects on the other mechanical properties is of a particular interest of researchers. Carbon black (CB) is known as an effective additive, generally improves the electrical conductivity of the composite materials [39]. The Nano-sized and non-crystalline CB have also been applied in the form of porous and/or compacted masses to enhance the overall mechanochemical properties of the structural ceramics [39–42]. CB has also shown promising outcomes in improving the thermal shock resistance of UHTCs [42]. It has been reported that the addition of 5 wt% carbon black increases the density of the sintered samples from 90% to 96%, and leads to a considerable reduction in the grain coarsening (from 5–30 μm to 1–8 μm) as well as the elimination of the oxide layers [14]. The improved densification behavior of the CB-doped ZrB_2-based composites has been observed to be 87% to 94% using 0 to 4 wt% CB, respectively. However, higher fractions (10 wt%) of CB have been reported to negatively affect the density of the samples [15].

However, whereas many inspiring works have been carried out on CB-doped ZrB_2-SiC composites, the role of CB on densification and mechanical behavior of ZrB_2-TiC composites has strangely discarded, except some published studies on self-propagating high-temperature synthesis (SHS) and hot pressing (HP) of the mentioned composite system. Therefore, this research is dedicated to investigating the role of CB on the densification behavior and mechanical properties of ZrB_2-TiC composites produced by the spark plasma sintering.

2. Experimental

2.1. Materials and methods

ZrB_2, TiC, and carbon black powders were used as the raw materials. The specification of the raw materials is presented in Table 1.

The raw powders were initially weighed to achieve the predesigned mixtures, according to Table 2. The powders were then separately dispersed in ethanol and consequently ultrasonicated (Daihan WUC-D10H, China) for 60 minutes. The mixing process was performed in the mentioned ultrasonic bath for 30 min and the obtained homogenous mixtures were stirred and dehydrated using a magnetic heater/stirrer (MR 3001K, Heidolph, Germany). The final drying process was

Table 1. The specifications of the raw materials.

Material	Average particle size	Purity (%)	Supplier
ZrB_2	< 5 µm	99.9	Xuzhou Hongwu Co. China
TiC	1–3 µm	99.5	Xuzhou Hongwu Co. China
Carbon black	~15 nm	> 95	US Research Nanomaterials

then carried out in an oven dryer (German Memmert Universal Oven) for 12 hours.

The obtained dry powder mixtures were crushed in a mortar and then passed through a 100-mesh sieve to avoid any agglomeration. In due course, the resultant powder mixtures were loaded into a graphite die (30 mm in diameter) covered by a 100 µm-thick graphite foil. Fig. 1 which shows the scanning electron microscopy (SEM) images of the powder mixtures of the samples confirms the particle size and homogenous distribution of the raw powders. It should be noted that the carbon black particles cannot be individually distinguished to their small (nano) size and the magnification of the SEM images.

The powder-contained die was then loaded into a spark plasma sintering furnace (Nanozint 10i, Khala Pooshan Felez Co., Iran). The SPS process parameters were set at the sintering temperature of 1900 °C, applied pressure of 40 MPa, and the dwelling time of 7 min.

2.2. Characterization

The disk-shaped obtained samples were de-graphitized via a diamond grinding wheel and polished to the 3000 mesh via SiC sand papers. The bulk (BD) and theoretical density (TD) of the SPSed samples were measured according to the Archimedes' principles and the rule of mixtures, respectively. Distilled water was used as the immersion media and the theoretical densities of ZrB_2, TiC, and carbon black were considered 6.1, 4.9, and 1.86 g/cm^3, respectively, for density calculations [43]. The relative density (RD) of the SPSed samples was finally calculated based on the obtained BD and TD.

The Mechanical properties of the SPSed samples (hardness and fracture toughness) were measured using a Vickers hardness apparatus (KM2/01-92123, Koopa Pazhoohesh, Iran). The diameters of at least three successful indents at the load of 49 N on the polished surface of the samples were measured to calculate the average Vickers hardness of the obtained sintered composites. The lengths of the radial cracks of the indents' projected area were also measured using an optical microscopy (Olympus X50, Japan), to calculate the indentation fracture toughness (IFT) of the samples, according to the Anstis' formula [44]:

Table 2. The labeling system of the samples based on the fraction of the raw materials.

Code	Fraction of the raw materials
ZT	80 vol% ZrB_2 and 20 vol% TiC
ZTCB	80 vol% ZrB_2, 20 vol% TiC, and 1 wt% (~3 vol%) carbon black

$$K_{IC} = (0.016 \pm 0.004)\left[\frac{E}{H_V}\right]^{1.2}\left[\frac{P}{C^{3.2}}\right] \quad (1)$$

where, E shows the elastic modulus of the porous body (in GPa), P shows the applied load on the indenter (in N), C is the average length of the radial cracks (in µm), and the indentation fracture toughness (K_{IC}) is calculated in MPa.m$^{0.5}$. The elastic modulus of the material (E) was also calculated using the Nielsen formula [45].

The microstructural and fractographical investigations of the SPSed samples were carried out using a field-emission scanning electron microscopy (FESEM, Mira3 Tescan, Czech Republic) equipped with an energy dispersive spectroscopy detector (EDS, DXP-X10P). The phase analysis of the samples was also performed by an X-ray diffraction spectrometer (XRD, Philips PW1730).

3. Results and discussion

3.1. Densification behavior and microstructural investigations

According to the density calculations, both of the samples have been fully densified (RD of 99.93% for ZT and 100% for ZTCB samples, respectively). Hence, it seems that the sintering process has been favorably progressed. The phase analysis of the samples, however, can provide better understanding of the sintering behavior and mechanisms. The XRD patterns of the sintered samples as well as the initial ZrB_2 and TiC powders are presented in Fig. 2.

As seen in the XRD patterns of Fig. 2, both of the sintered samples have developed a microstructure majorly including the $(Zr,Ti)B_2$ phase or in the other word, a solid solution of TiB_2 in ZrB_2. However, the larger volume fraction of the carbon sources (CB and TiC) in the ZTCB sample has resulted in the higher fraction of synthesized ZrC, according to the intensity of ZrC peaks in the ZTCB XRD pattern. On

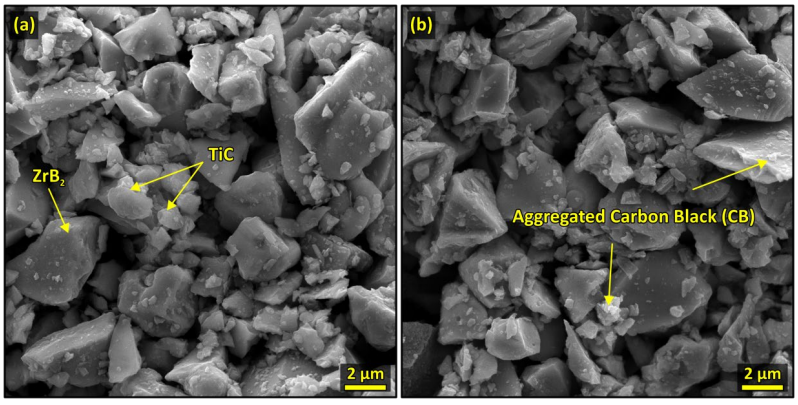

Fig. 1. The SEM images of the raw powder mixtures of a) ZT and b) ZTCB samples.

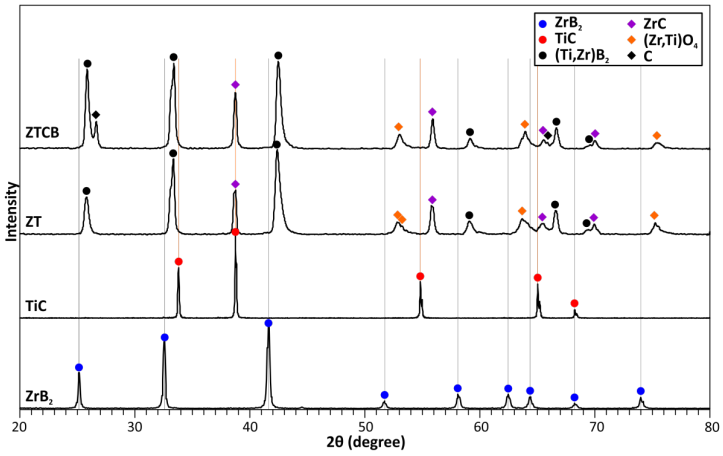

Fig. 2. The XRD patterns of the sintered samples compared to the raw powders.

the other hand, the volume fraction of the complex oxide impurities ($(Zr,Ti)O_4$ phase)has slightly decreased in the sample contained CB. It is also worthy to note that whereas no free-carbon-related peak is detected in ZT sample, ZTCB sample shows the detectable amounts of free carbon in its final microstructure. The peaks of the crystalline carbon can be attributed to the crystallization of the remained amorphous carbon through the high-temperature and pressurized sintering process. Such a phenomenon has been widely observed and reported previously [13]. Based on the XRD patterns, the formation of ZrC in both of the samples is clearly confirmed, as previously reported by Mishra et al. [15]. The higher volume fraction of the ZrC synthesized in the ZTCB sample is confirmed on the basis of the greater intensity and width of the ZrC peaks in the XRD pattern of the sample. Undoubtedly, this can be considered because of the higher amount of carbon available from the two carbon sources in the ZTCB sample.

The manifestation of $(Zr,Ti)B_2$ peaks in both of the samples addresses the dissolution of TiB_2 in the solid solution. Particularly, as the overall peak alignment of the $(Zr,Ti)B_2$ phase resembles the standard XRD pattern of ZrB_2 with shifts in the peak positions, the dissolution of TiB_2 can be confirmed. Titanium diboride is reported as a byproduct of ZrC synthesis through the following reaction [14]:

$$ZrB_2 + TiC \rightarrow TiB_2 + ZrC \quad (2)$$

Hence, as the reaction takes place at the interface of ZrB_2/TiC particles, the synthesized TiB_2 can easily dissolve in the ZrB_2 matrix through the

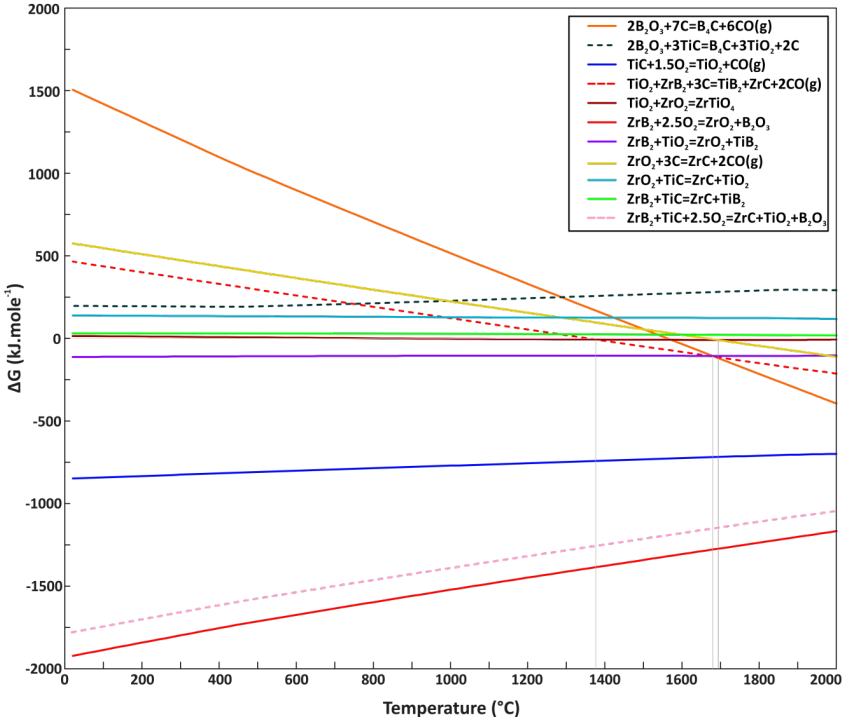

Fig. 3. The variations of Free Gibbs Energy vs. temperature for some of the possible chemical reactions in the system. Thermodynamic calculations are carried out using HSC Chemistry package.

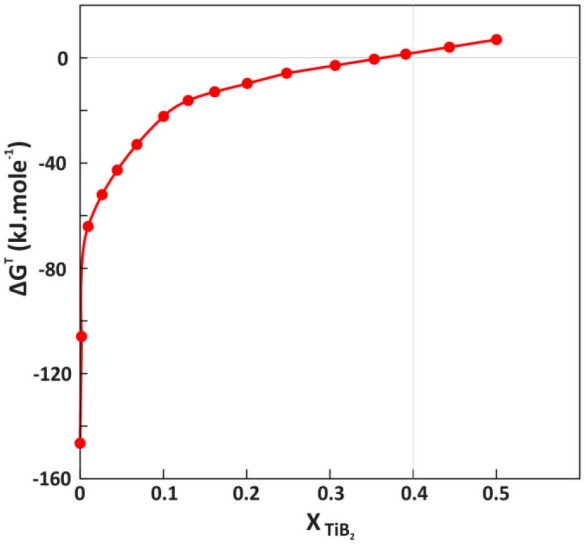

Fig. 4. The variations of ΔG^T vs. the fraction of synthesized and dissolved TiB_2 in ZrB_2 matrix, according to Eq. 11.

replacement of zirconium atoms with smaller titanium ones. The dissolution phenomenon is also promoted by relatively similar crystalline structure of both phases and not only leads to a uniform distribution of Ti in the solid solution but also results in compressive stresses in ZrB_2 crystals. The compressive stresses cause the decreased lattice parameter of ZrB_2 and consequently reduce the distance between crystal plans which is manifested as peak shift in XRD patterns. Such a peak shifting phenomenon, may be intensified via increased Ti dissolution, and finally leads to the appearance of individual $(Zr,Ti)B_2$ peaks, as seen in Fig. 2. However, it should be noted that as the dissolution takes place in ZrB_2 crystals, the XRD pattern of $(Zr,Ti)B_2$ solid solution follows the overall feature of ZrB_2 XRD pattern.

The thermodynamic calculations of the possible chemical reactions can provide better understanding about the mechanism of reactive sintering as well as the densification behavior of the SPSed composites. Hence, the variations of Free Gibbs Energy (FGE) vs. temperature for the possible chemical reactions in the composite system are presented as ΔG vs. T curves in Fig. 3.

According to Fig. 3, many of the chemical reactions seem not to be thermodynamically favorable, as their ΔG values do not fulfill the energy term of the reaction (positive ΔG). On contrary, the oxidation of ZrB_2 and TiC compounds (Eqs. 3 and 4, respectively) is thermodynamically possible through all the temperature ranges.

$$ZrB_2 + 2.5O_2(g) \rightarrow ZrO_2 + B_2O_3 \quad (3)$$

$$TiC + 1.5O_2(g) \rightarrow TiO_2 + CO(g) \quad (4)$$

ZrB_2 may also react with TiO_2 through the following reaction which results in the formation of TiB_2 and ZrO_2:

$$ZrB_2 + TiO_2 \rightarrow ZrO_2 + TiB_2 \quad (5)$$

Therefore, it seems that the C. according to Fig. 3, carbon can favorably react with B_2O_3 and form boron carbide through the following reaction:

$$2B_2O_3 + 7C \rightarrow B_4C + 6CO(g) \quad (6)$$

The synthesis of TiB_2 which is favorably occurred through Eq. 5 at temperatures below 1700 °C, would then continue through the following reaction:

$$ZrB_2 + TiO_2 + 3C \rightarrow TiB_2 + ZrC + 2CO(g) \quad (7)$$

It should be noted that although the energy term is more favorable for Eq. 6, the occurrence and progression of the mentioned reaction are tightly restricted by the available B_2O_3, which is known as the most volatile compound of the system and majorly drawn out via the applied vacuum of the SPS chamber. Therefore, as presented in Fig. 2, no peak of B_4C is found in the XRD patterns of both samples; although the presence of detectable amounts of boron carbide is thermodynamically expected.

While TiC is the only carbon source of ZT sample, in ZTCB sample, the presence of carbon black promotes the progression of Eq. 7 and leads to intensified ZrC formation. As seen in Fig. 2, the volume fraction (intensity and width of the peaks) of $ZrTiO_4$ phase has also decreased in CB-contained sample, which can be attributed to the intensified chemical reduction of the formed oxides via carbon black. However, the in-situ synthesis of ZrC phase in ZT sample is thermodynamically favorable through the following chemical reaction:

$$ZrB_2 + TiC + 2.5O_2(g) \rightarrow ZrC + TiO_2 + B_2O_3 \quad (8)$$

As seen in Fig. 3, the chemical reaction of Eq. 8 follows the overall trend of Eq. 7. Hence, it can be paraphrased that the oxidation of ZrB_2 may simultaneously occur with the formation of ZrC. It is also worthy to note that while the chemical reaction of Eq. 7 is promoted according to the Le Chatelier's principle (drawn out of the formed CO through the vacuum chamber), it is tightly limited by the amount of TiO_2 in system. The formation of enough TiO_2 itself depends on the availability of oxygen (See Eq. 4) in the vacuum chamber. The chemical reaction of Eq. 8 is also restricted by the amount of available oxygen. Therefore, despite their favorable energy term, Eqs. 7 and 8 cannot play a major role in the ZrC formation through the SPS process.

On the other hand and based on Fig. 2, TiB_2 phase would be presented as a mixed crystal with ZrB_2. Hence, although the occurrence of Eq. 2 in its presented form seems to be thermodynamically unfavorable, the partial progression of this chemical reaction should be taken into account. Ivashchenko et al. [46] have modified the FGE balance of the reaction, according to the FGE variations of the solid solution formation. The variations of ΔG for the chemical reaction of Eq. 2 are calculated as Eq. 9:

$$ZrB_2 + TiC \rightarrow TiB_2 + ZrC \quad \Delta G^R = +19.32\ kJ \quad T = 1900\ °C \quad (9)$$

The reaction however includes the in-situ formation of ZrB_2/TiB_2 solid solution ($(Zr,Ti)B_2$ phase). Hence, the energy balance of the solid solution formation (Eq. 10) should also be taken into account:

$$ZrB_2 + \delta TiB_2 \rightarrow Ti_\delta ZrB_{2(1+\delta)} \quad \Delta G^{SS} = RT \ln\left(\frac{\alpha^{SS}TiB_2}{(\alpha TiB_2)^\delta . \alpha ZrB_2}\right) \quad (10)$$

And the total variations of the FGE for the simultaneous formation of ZrC and TiB_2 (Eq. 2) can be calculated according to Eq. 11:

$$\Delta G^T = \Delta G^R + \Delta G^{SS} \quad (11)$$

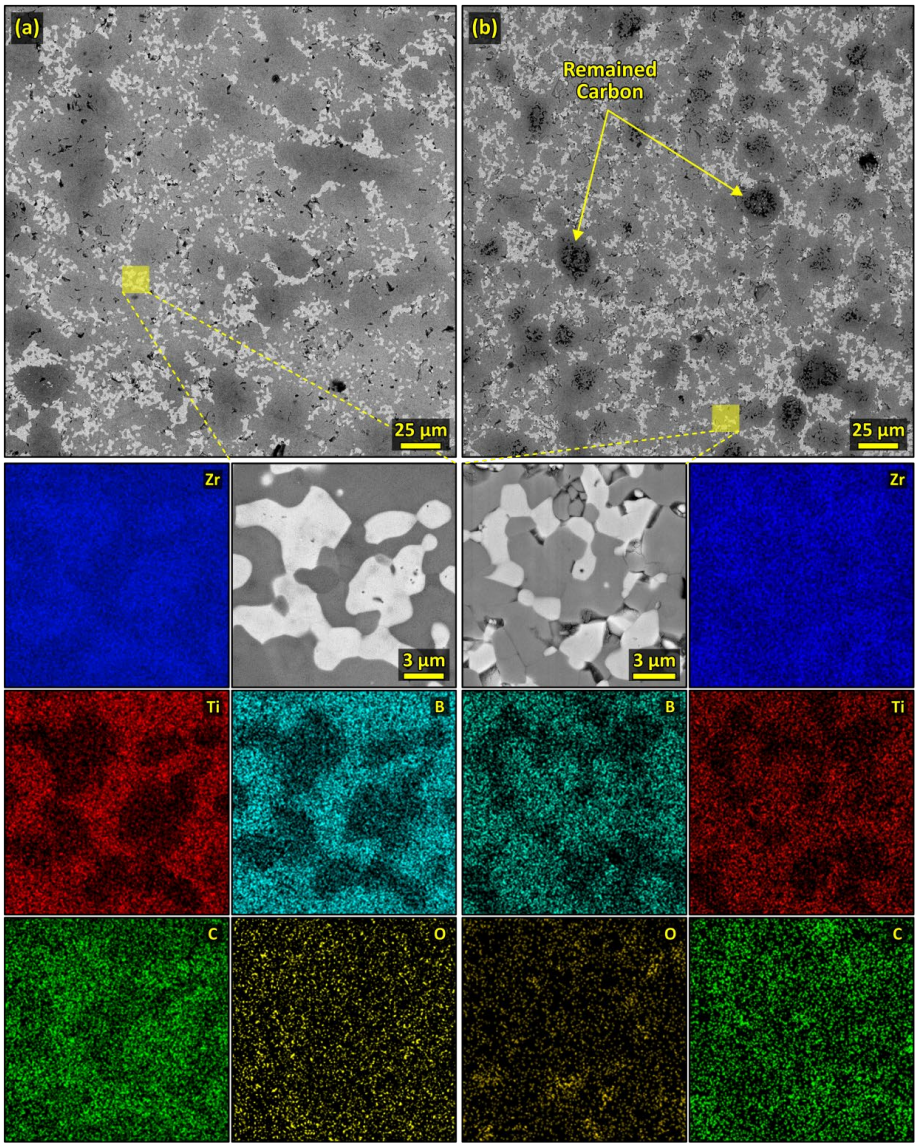

Fig. 5. FESEM micrographs and related EDS elemental maps of the selected area in a) ZT and b) ZTCB samples.

Within these equations, ΔG^{SS}, ΔG^{R}, ΔG^{T}, $\alpha^{SS}TiB_2$, αTiB_2, and αZrB_2 represent the ΔG of ZrB_2/TiB_2 solid solution formation, the ΔG of the reaction (Eq. 2) at the sintering temperature, the total (modified) ΔG of the chemical reaction of Eq. 2, the activity of TiB_2 in the crystal structure of ZrB_2 (solid solution), the activity of TiB_2, and the activity of ZrB_2, respectively. Fig. 4 shows the variation of ΔG^{T} vs. the fraction of synthesized and dissolved TiB_2. Considering the synthesized TiB_2 and initial ZrB_2 as pure phases, their activity in Eq. 10 would be equal to 1. However, when TiB_2 is dissolved in the ZrB_2 crystal, the activity of dissolved TiB_2 would depend on its mole fraction in the solid solution, which should be considered less than the ideal amount [46]. Hence, at the initial stages of TiB_2 synthesis and dissolution, the activity of the mixed TiB_2 should be very small, so the ΔG^{SS} would be considerably negative and cause negative ΔG^{T} (see Fig. 4). Hence, it can be concluded that while the direct reaction of ZrB_2 and TiC seems to be thermodynamically impossible in its standard form, the simultaneous dissolution of synthesized TiB_2 in ZrB_2 changes the energy term of the reaction and promote the progression of Eq. 2. As seen in Fig. 4, the energy term would be favorable till the fraction of dissolved TiB_2 reaches around 40 at% (50 wt%). Accompanied by the detection of $Zr_{0.5}Ti_{0.5}B_2$ peaks in the XRD patterns, the formation of considerable fractions of ZrC at both samples (with and without free carbon) also confirms the dominant role of modified Eq. 2 in the reactive sintering process, compared to Eq. 7. However, the lower fraction of $TiZrO_4$ as well as the slightly higher fraction of synthesized ZrC, addresses the reduction of ZrO_2 via free carbon in ZTCB sample, which occurs through the following reaction (particularly at T > 1750 °C, according to Fig. 3):

$$ZrO_2 + 3C \rightarrow ZrC + 2CO(g) \quad (12)$$

Fig. 5 shows the FESEM micrographs and related EDS elemental maps of the sintered samples. Accordingly, while the ZT sample shows a

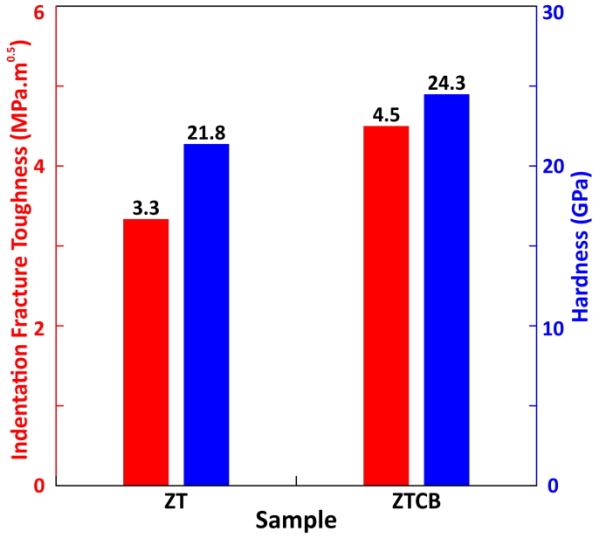

Fig. 6. The measured hardness and indention fracture toughness of the SPSed composite.

small fraction of the remained porosities (dark areas), the microstructure of the ZTCB sample also includes remained carbon (marked in Fig. 5b). Comparing the magnified area in both samples, relatively smoother and clearer interfaces between the synthesized ZrC and the matrix can also be observed in ZT sample. The microstructural images of Fig. 5, however, confirm the near-fully dense composite structures in both sintered samples.

In addition to the relatively homogenous phase distribution in the microstructure of the SPSed composites, comparing the elemental maps of Zr and Ti confirms the results of the XRD analysis about the formation of $(Zr,Ti)B_2$ as the continuous phase (matrix) in both of the composite samples. The Zr-rich areas in which the higher concentrations of Zr atoms can be observed through the elemental maps address the formation of ZrC phase (depleted of Ti atoms). Zirconium carbide, as previously reported [2], can be distinguished as light gray (white) area in the back-scattered electron micrographs. The ZrB_2-TiB_2 solid solutions are also observed as the dark gray areas, as shown in Fig. 5.

Both of the samples include areas with high oxygen concentrations, although the oxides are better distinguished in ZTCB sample near the remained carbon and/or porosities. The presence of such oxides in the interfaces and particularly in triple points, confirms the presence of previously addressed $ZrTiO_4$ phase. However, comparing the EDS elemental maps of C and O, the consumption of the oxides through the reduction reaction and the formation of secondary ZrC phase in ZTCB sample is confirmed. Such a phenomenon seems to cause discontinued interfaces in the mentioned sample, compared to the ZT sample.

3.2. Mechanical properties

Fig. 6 shows the measured hardness and indentation fracture toughness (IFT) values of the SPSed composites. While the obtained hardness of the current TiC-reinforced composites is close to the overall reports of ZrB_2-SiC composites, the relatively increased hardness of the ZTCB sample (24.3 MPa) attracts more attention. Farahbakhsh et al. [47] investigated the ZrB_2-SiC composite doped with nano-sized carbon black particles densified through hot-pressing (HP) at 1850 °C under the applied pressure of 20 MPa for 60 min. They found that the addition of 20 vol% SiC and 10 vol% nano-sized carbon black can lead to a relative density of 99.8%, a Vickers hardness of 16.7 GPa, and a fracture toughness of 5.8 $MPa.m^{0.5}$. Zhou et al. [48] investigated the HPed ZrB_2-20 vol% SiC composites doped with 5 vol% nano-sized carbon black densified at 1900 °C, and reported a hardness of 12.3 GPa and a fracture toughness of 6.6 $MPa.m^{0.5}$ [48]. Accordingly, while the presence of carbon black may lead to the relatively higher volume fraction of the porosities as well as the remained carbon (as the soft interfacial phase) in the final microstructure of the ZTCB sample, the higher hardness number of this sample can be attributed to the role of CB in ZrO_2 reduction, which leads to the higher volume fraction of in-situ synthesized ZrC. The formation of B_4C as a result of the reaction between carbon and B_2O_3 impurity (Eq. 6), although has not been clearly confirmed (but thermodynamically favorable at higher temperature), may be considered as another effective parameter in achieving such a relatively high hardness number.

Compared to the common ZrB_2-SiC composites with similar volume fractions of the reinforcement phase, the formation of $(Zr,Ti)B_2$ solid solution as the matrix of the composites in this study, can be considered the main hardening mechanism. The formation of in-situ ZrC and B_4C as the hard secondary phases also promotes the enhanced hardness of the composites. The formation of such an addressed solid solution, however, leads to the highly stressed (compressive) matrix and then, would influence the fracture toughness of the materials. In addition to the formation of a solid solution as the matrix, the toughening behavior of the sintered composites is also affected by the secondary phases and reinforcements.

Increased fracture toughness via the secondary phases mainly occurs through the interactions of the progressing cracks including crack deflection and bridging with these phases. Through such mechanisms, the concentrated stress at the crack tip would be released and lead to improving fracture toughness. However, such mechanisms are highly dependent on the type and quality of the interfaces between the secondary phases and the matrix [41, 42].

The FESEM micrographs and corresponding EDS elemental maps of the sintered samples are presented in Fig. 7 to illustrate the fracture behavior and phase distribution in the samples.

As seen in Fig. 7, the fracture surface of the ZT sample shows relatively large fracture plans (marked areas with dashes) in both of the matrix and reinforcement phases (dark and light gray areas in Fig. 7b, respectively) and resembles the smooth fracture surface. On contrary, ZTCB sample includes a relatively rough fracture surface. In other words, whereas several changes in the fracture plan are observed in ZTCB sample and shows a prolonged crack path through intergranular fracture mode, transgranular fracture mode with relatively smooth surfaces is observed in ZT sample. Hence, as seen in Fig. 6, higher IFT value is observed in ZTCB sample, which is derived from the prolonged intergranular crack path. The presence of secondary phases (mainly ZrC and remained carbon) is also confirmed according to the magnified area in Fig. 7b and its related EDS elemental maps. Fig. 8 also shows the FESEM micrographs of the propagation of the cracks induced by the Vickers indenter in both of the sintered composite samples, and can be used to reveal the dominant toughening mechanisms in the materials.

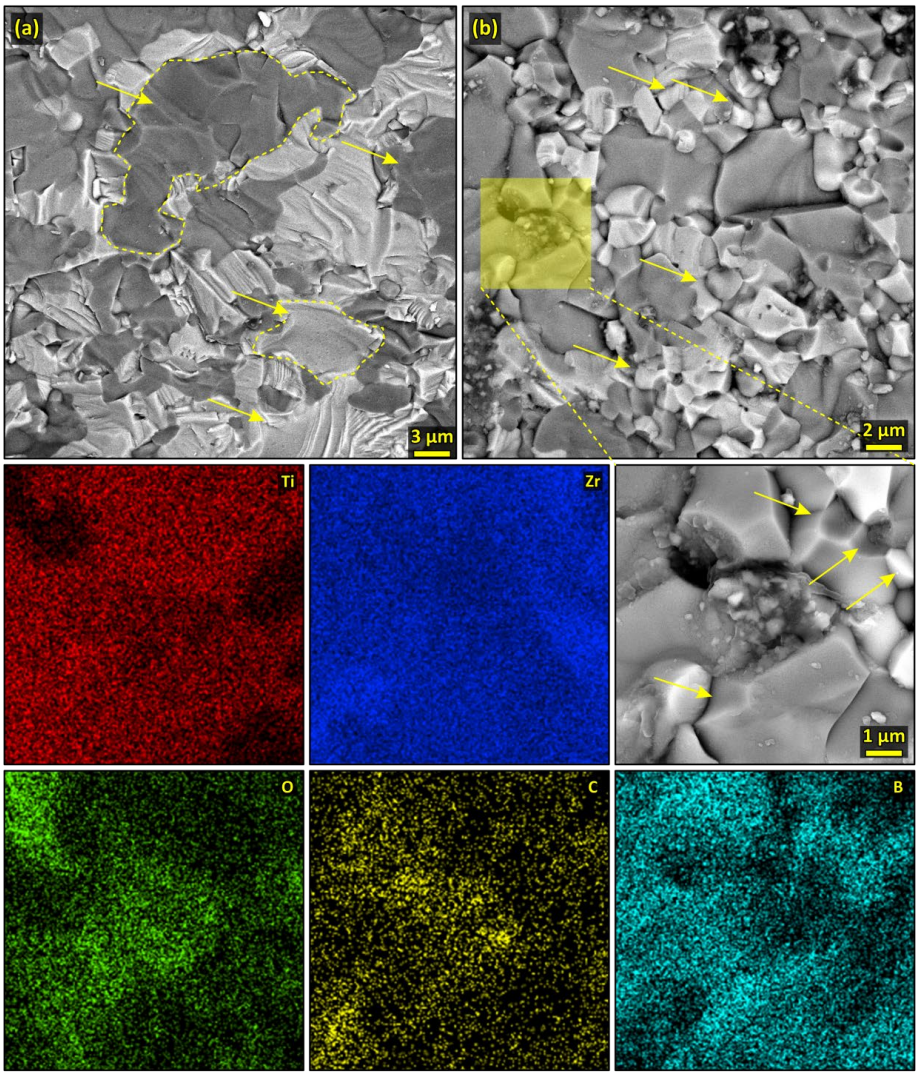

Fig. 7. The FESEM micrographs of the fracture surface in a) ZT and b) ZTCB sample with the related EDS elemental maps.

As seen in Fig. 8, the cracks are propagating in relatively direct paths in ZT sample, which shows the minimum effects of the reinforcement in toughening the composite. In other words, the formation of the solid solution plays the major role in toughening the ZT sample. Through such a mechanism, the intrinsic strength of the highly stressed (compressive) solid solution matrix blunts the crack tip and inhibits the fast propagation of the cracks. However, the reinforcements also may participate in the toughening of the composite through various mechanisms like crack deflection, as marked in Fig. 8a-1. Such a behavior can be attributed to the synthesis mechanism of the reinforcements in ZT sample in which the in-situ synthesized ZrC is mainly formed through the simultaneous synthesis and dissolution of TiB_2 (Eq. 3). Hence, while clear interfaces would be formed at the inter-phase boundaries, the concentrated stresses at the interfaces would be at the minimum level (to keep the lattice mismatch energy at the lowest level, and promotes the simultaneous dissolution of TiB_2 and the synthesis of ZrC). Therefore, the ability of the formed interfaces to effectively blunt or deflect the propagating cracks would be decreased. Hence, the toughening through secondary phases is not the dominant toughening mechanism in ZT sample, compared to the solid solution forming in the matrix which resulted in branching and blunting the cracks (Fig. 8b-1). The relatively smooth fracture surface of the ZT sample (Fig. 7a) in which no obvious difference is observed between the matrix and the in-situ synthesized secondary phases (ZrC), confirms such a discussion.

The addition of carbon black, however, changes the toughening behavior of the composite. As seen in Fig. 8b, the paths of the propagating cracks include several deflections, mainly at the inter-phase boundaries. Zhou et al. [48] manufactured a ZrB_2-based composite reinforced with 20 vol% SiC and 5 vol% of carbon black through the hot pressing, and measured the fracture toughness of 6.6 $MPa.m^{0.5}$. They concluded that the increase in the fracture toughness is induced by the weak interfaces, which results in the formation of micro-cracks. Such micro-cracks activate a number of toughening mechanisms including crack deflection, blunting, and bridging. Fig. 8b confirms the occurrence of similar mechanisms in ZTCB samples. As shown in Figs. 8b-1 and 8b-2, while the inter-phase boundaries in ZT sample have not effectively participated in crack

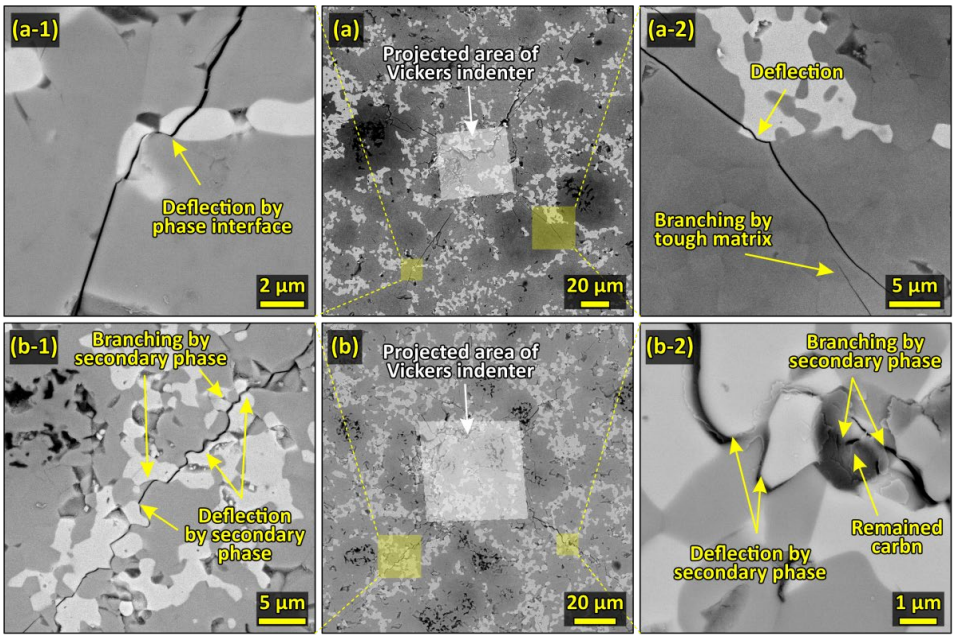

Fig. 8. The FESEM micrographs of the cracks induced by the Vickers indenter in a) ZT and b) ZTCB samples.

deflection, the crack path has repeatedly changed at the interfaces between ZrC and the matrix in ZTCB sample. Hence, besides the increased strength of the matrix induced by the solid solution formation, the relatively weak inter-phase boundaries which may include the remained carbon (See Fig. 8b-2), participates in the toughening of ZTCB sample and lead to the obtained fracture toughness, which shows approximately 30% increase compared to carbon-free sample (ZT). The formation of secondary ZrC (the product of ZrO2 reduction via carbon black through Eq. 12) may also promote the increased fracture toughness in ZTCB sample, as these types of ZrC form different types of interfaces with the matrix.

It is also worthy to note that while no traces of B_4C was found in both of the phase analysis and microstructural investigations, the possible presence of boron carbide nanoparticles at the interfaces of the ZTCB sample may also promote crack deflection at the boundaries of the in-situ synthesized ZrC. The remained carbon which is presented in the microstructure as a porous secondary phase, may also influence the crack blunting and crack deflection mechanism, and consequently enhance the fracture toughness of the composite (marked in Fig. 8b-2). Conclusively, while the increased strength of the matrix due to solid solution formation is introduced as the main toughening mechanism of ZT sample, the addition of carbon black activates the interface-induced toughening mechanisms such as crack deflection and branching, and leads to the enhanced fracture toughness a CB-contained ZrB_2-TiC composite sample.

4. Conclusions

The effects of nano-sized carbon black on the mechanical properties, phase arrangement, and microstructural characteristics of ZrB_2-TiC ceramics densified through spark plasma sintering at 1900 °C for 7 minutes and under the applied pressure of 40 MPa were studied.

The obtained results revealed higher hardness and considerable improvement in the fracture toughness, using 1 wt% of nano-sized carbon black as the additive in ZrB_2-20 vol% TiC composites. The formation of $(Zr,Ti)B_2$ solid solution as the matrix and in-situ synthesized ZrC as the reinforcement was confirmed through the characterization of the sintered materials. The thermodynamic of reactive sintering and solid solution formation as well as the phase arrangements of the composites with and without carbon black additive were then investigated.

It was also found that while the carbon black does not meaningfully affect the densification behavior of the composite, it can activate several toughening mechanisms and besides the hardness, enhances the fracture toughness of the ZrB_2-TiC composites densified through spark plasma sintering. The toughening mechanisms and the fracture behavior of the composites were also discussed.

CRediT authorship contribution statement

Hamid Istgaldi: Writing – original draft, Investigation, Methodology.
Mehdi Mehrabian: Writing – original draft, Data curation.
Faramarz Kazemi: Writing – original draft, Validation.
Behzad Nayebi: Writing – review & editing, Visualization, Supervision, Project administration.

Data availability

The data underlying this article will be shared on reasonable request to the corresponding author.

Declaration of competing interest

The authors declare no competing interests.

Funding and acknowledgment

The content of this article is based on the master thesis of the first author, which was approved under thesis contract number 963 dated 12-12-2018 at the University of Mohaghegh Ardabili (Iran). The authors wish to express their gratitude to the staff of the Materials and Energy Research Center (Karaj, Iran) for their invaluable support and guidance during the implementation of this project.

References

[1] S.-Q. Guo, Densification of ZrB2-based composites and their mechanical and physical properties: a review, J. Eur. Ceram. Soc. 29 (2009) 995–1011. https://doi.org/10.1016/j.jeurceramsoc.2008.11.008.

[2] H. Istgaldi, M. Shahedi Asl, P. Shahi, B. Nayebi, Z. Ahmadi, Solid solution formation during spark plasma sintering of ZrB2–TiC–graphite composites, Ceram. Int. 46 (2020) 2923–2930. https://doi.org/10.1016/j.ceramint.2019.09.287.

[3] Z. Balak, M. Shahedi Asl, M. Azizieh, H. Kafashan, R. Hayati, Effect of different additives and open porosity on fracture toughness of ZrB2–SiC-based composites prepared by SPS, Ceram. Int. 43 (2017) 2209–2220. https://doi.org/10.1016/j.ceramint.2016.11.005.

[4] M. Vajdi, F.S. Moghanlou, E.R. Niari, M. Shahedi Asl, M. Shokouhimehr, Heat transfer and pressure drop in a ZrB2 microchannel heat sink: a numerical approach, Ceram. Int. 46 (2020) 1730–1735. https://doi.org/10.1016/j.ceramint.2019.09.146.

[5] M. Jaberi Zamharir, M. Shahedi Asl, N. Pourmohammadie Vafa, M. Ghassemi Kakroudi, Significance of hot pressing parameters and reinforcement size on densification behavior of ZrB2–25 vol% SiC UHTCs, Ceram. Int. 41 (2015) 6439–6447. https://doi.org/10.1016/j.ceramint.2015.01.082.

[6] H. Istgaldi, B. Nayebi, Z. Ahmadi, P. Shahi, M. Shahedi Asl, Characterization of ZrB2–TiC composites reinforced with short carbon fibers, Ceram. Int. 46 (2020) 23155–23164. https://doi.org/10.1016/j.ceramint.2020.06.095.

[7] V.H. Nguyen, S.A. Delbari, M. Shahedi Asl, Q. Van Le, A.S. Namini, et al. Combined role of SiC whiskers and graphene nano-platelets on the microstructure of spark plasma sintered ZrB2 ceramics, Ceram. Int. 47 (2021) 12459–12466. https://doi.org/10.1016/j.ceramint.2021.01.103.

[8] B. Mohammadzadeh, S. Jung, T.H. Lee, J.H. Cha, J. Park, et al., Characterization and FEA evaluation of a ZrB2-SiC ceramic containing TaC for beam–column joint application. Ceram, Int. 47 (2020) 11438–11450. https://doi.org/10.1016/j.ceramint.2020.12.271.

[9] V.H. Nguyen, M. Shahedi Asl, S.A. Delbari, Q. Van Le, A.S. Namini, et al., Effects of SiC on densification, microstructure and nano-indentation properties of ZrB2–BN composites, Ceram. Int. 47 (2020) 9873–9880. https://doi.org/10.1016/j.ceramint.2020.12.129.

[10] M.D. Alvari, M.G. Kakroudi, B. Salahimehr, R. Alaghmandfard, M. Shahedi Asl, M. Mohammadi, Microstructure, mechanical properties, and oxidation behavior of hot-pressed ZrB2–SiC–B4C composites, Ceram. Int. 47 (2020) 9627–9634. https://doi.org/10.1016/j.ceramint.2020.12.101.

[11] M. Shahedi Asl, M. Ghassemi Kakroudi, S. Noori, Hardness and toughness of hot pressed ZrB2–SiC composites consolidated under relatively low pressure, J. Alloys Compd. 679 (2015) 481–487. https://doi.org/10.1016/j.jallcom.2014.09.006.

[12] M. Shahedi Asl, M. Ghassemi Kakroudi, A processing–microstructure correlation in ZrB2–SiC composites hot-pressed under a load of 10 MPa, Univers. J. Mater. Sci. 3 (2015) 14–21. https://www.hrpub.org/journals/article_info.php?aid=2325.

[13] M. Shahedi Asl, B. Nayebi, Z. Ahmadi, M.J. Zamharir, M. Shokouhimehr, Effects of carbon additives on the properties of ZrB2–based composites: a review, Ceram. Int. 44 (2018) 7334–7348. https://doi.org/10.1016/j.ceramint.2018.01.214.

[14] S.K. Mishra, S.K. Das, Sintering and microstructural behaviour of SHS produced zirconium diboride powder with the addition of C and TiC, Mater. Lett. 59 (2005) 3467–3470. https://doi.org/10.1016/j.matlet.2005.06.015.

[15] S.K. Mishra, L.C. Pathak, Effect of carbon and titanium carbide on sintering behaviour of zirconium diboride, J. Alloys Compd. 465 (2008) 547–555. https://doi.org/10.1016/j.jallcom.2007.11.004.

[16] J. Yin, H. Zhang, Y. Yan, Z. Huang, X. Liu, D. Jiang, High toughness in pressureless densified ZrB2-based composites co-doped with boron–titanium carbides, Scr. Mater. 66 (2012) 523–526. https://doi.org/10.1016/j.scriptamat.2011.12.036.

[17] M. Sribalaji, B. Mukherjee, S.R. Bakshi, P. Arunkumar, K.S. Babu, A.K. Keshri, In-situ formed graphene nanoribbon induced toughening and thermal shock resistance of spark plasma sintered carbon nanotube reinforced titanium carbide composite, Compos. B. Eng. 123 (2017) 227–240. https://doi.org/10.1016/j.compositesb.2017.05.035.

[18] J.X. Xue, J.X. Liu, G.J. Zhang, H.B. Zhang, T. Liu, et al., Improvement in mechanical/physical properties of TiC-based ceramics sintered at 1500 °C for inert matrix fuels, Scr. Mater. 114 (2016) 5–8. https://doi.org/10.1016/j.scriptamat.2015.11.024.

[19] D. Chen, W. Li, X. Zhang, P. Hu, J. Han, C. Hong, W. Han, Microstructural feature and thermal shock behavior of hot-pressed ZrB2–SiC–ZrO2 composite, Mater. Chem. Phys. 116 (2009) 348–352. https://doi.org/10.1016/j.matchemphys.2009.03.033.

[20] G.J. Zhang, Z.Y. Deng, N. Kondo, J.F. Yang, T. Ohji, Reactive hot pressing of ZrB2–SiC composites, J. Am. Ceram. Soc. 83 (2000) 2330–2332. https://doi.org/10.1111/j.1151-2916.2000.tb01558.x.

[21] H. Wang, C. Wang, X. Yao, D. Fang, Processing and Mechanical Properties of Zirconium Diboride-Based Ceramics Prepared by Spark Plasma Sintering, J. Am. Ceram. Soc. 90 (2007) 1992–1997. https://doi.org/10.1111/j.1551-2916.2007.01665.x.

[22] F. Guillard, A. Allemand, J.D. Lulewicz, J. Galy, Densification of SiC by SPS-effects of time, temperature and pressure, J. Eur. Ceram. Soc. 27 (2007) 2725–2728. https://doi.org/10.1016/j.jeurceramsoc.2006.10.005.

[23] Z. Balak, M. Azizieh, H. Kafashan, M. Shahedi Asl, Z. Ahmadi, Optimization of effective parameters on thermal shock resistance of ZrB2-SiC-based composites prepared by SPS: Using Taguchi design, Mater. Chem. Phys. 196 (2017) 333–340. https://doi.org/10.1016/j.matchemphys.2017.04.062.

[24] E. Ghasali, H. Nouranian, A. Rahbari, H. Majidian, M. Alizadeh, T. Ebadzadeh, Low temperature sintering of aluminum-zircon metal matrix composite prepared by spark plasma sintering, Mater. Res. 19 (2016) 1189–1192. https://doi.org/10.1590/1980-5373-MR-2016-0395.

[25] A.L. Chamberlain, W.G. Fahrenholtz, G.E. Hilmas, Pressureless sintering of zirconium diboride, J. Am. Ceram. Soc. 89 (2006) 450–456. https://doi.org/10.1111/j.1551-2916.2005.00739.x.

[26] A. Balbo, D. Sciti, Spark plasma sintering and hot pressing of ZrB2–MoSi2 ultra-high-temperature ceramics, Mater. Sci. Eng. 475 (2008) 108–112. https://doi.org/10.1016/j.msea.2007.01.164.

[27] M. Shahedi Asl, B. Nayebi, Z. Ahmadi, P. Pirmohammadi, M. Ghassemi Kakroudi, Fractographical characterization of hot pressed and pressureless sintered SiAlON-doped ZrB2–SiC composites, Mater. Charact. 102 (2015) 137–145. https://doi.org/10.1016/j.matchar.2015.03.002.

[28] S.R Levine, E.J. Opila, M.C. Halbig, J.D. Kiser, M. Singh, J.A. Salem, Evaluation of ultra-high temperature ceramics for aero-propulsion use, J. Eur. Ceram. Soc. 22 (2002) 2757–2767. https://doi.org/10.1016/S0955-2219(02)00140-1.

[29] M. Shahedi Asl, M.G. Kakroudi, R.A. Kondolaji, H. Nasiri, Influence of graphite nano-flakes on densification and mechanical properties of hot-pressed ZrB2–SiC composite, Ceram. Int. 41 (2015) 5843–5851. https://doi.org/10.1016/j.ceramint.2015.01.014.

[30] Z. Ahmadi, B. Nayebi, M. Shahedi Asl, M.G. Kakroudi, Fractographical characterization of hot pressed and pressureless sintered AlN-doped ZrB2–SiC composites, Mater. Charact. 110 (2015) 77–85. https://doi.org/10.1016/j.matchar.2015.10.016.
[31] M. Shahedi Asl, M.G. Kakroudi, Characterization of hot-pressed graphene reinforced ZrB2–SiC composite, Mater. Sci. Eng. 625 (2015) 385–392. https://doi.org/10.1016/j.msea.2014.12.028.
[32] W. Zhi, W. Zhanjun, S. Guodong, Fabrication, mechanical properties and thermal shock resistance of a ZrB2-graphite ceramic, Int. J. Refract. Met. Hard Mater. 29 (2011) 351–355. https://doi.org/10.1016/j.ijrmhm.2010.12.014.
[33] Z. Wang, S. Wang, X. Zhang, P. Hu, W. Han, C. Hong, Effect of graphite flake on microstructure as well as mechanical properties and thermal shock resistance of ZrB2–SiC matrix ultrahigh temperature ceramics, J. Alloys Compd. 484 (2009) 390–394. https://doi.org/10.1016/j.jallcom.2009.04.109.
[34] X. Zhang, Z. Wang, X. Sun, W. Han, C. Hong, Effect of graphite flake on the mechanical properties of hot pressed ZrB2–SiC ceramics, Mater. Lett. 62 (2008) 4360–4362. https://doi.org/10.1016/j.matlet.2008.07.027.
[35] W.B. Tian, Y.M. Kan, G.J. Zhang, P.L. Wang, Effect of carbon nanotubes on the properties of ZrB2–SiC ceramics, Mater. Sci. Eng. 487 (2008) 568–573. https://doi.org/10.1016/j.msea.2007.11.027.
[36] G.B. Yadhukulakrishnan, S. Karumuri, A. Rahman, R.P. Singh, A.K. Kalkan, S.P. Harimkar, Spark plasma sintering of graphene reinforced zirconium diboride ultra-high temperature ceramic composites, Ceram. Int. 39 (2013) 6637–6646. https://doi.org/10.1016/j.ceramint.2013.01.101.
[37] F. Yang, X. Zhang, J. Han, S. Du, Characterization of hot-pressed short carbon fiber reinforced ZrB2–SiC ultra-high temperature ceramic composites, J. Alloys Compd. 472 (2009) 395–399. https://doi.org/10.1016/j.jallcom.2008.04.092.
[38] Z. Nasiri, M. Mashhadi, A. Abdollahi, Effect of short carbon fiber addition on pressureless densification and mechanical properties of ZrB2–SiC–Csf nanocomposite, Int. J. Refract. Met. Hard Mater. 51 (2015) 216–223. https://doi.org/10.1016/j.ijrmhm.2015.04.005.
[39] W. Wang, K. Cann, Carbon black used as a fluidization aid in gas phase elastomer polymerization: I. Carbon black–monomer interactions, Carbon. 40 (2002) 221–224. https://doi.org/10.1016/S0008-6223(01)00178-6.
[40] C.M. Long, M.A. Nascarella, P.A.Valberg, Carbon black vs. black carbon and other airborne materials containing elemental carbon: physical and chemical distinctions, Environ. Pollut. 181 (2013) 271–286. https://doi.org/10.1016/j.envpol.2013.06.009.
[41] K.H. Wu, T.H. Ting, G.P. Wang, W.D. Ho, C.C. Shih, Effect of carbon black content on electrical and microwave absorbing properties of polyaniline/carbon black nanocomposites, Polym. Degrad. Stab. 93 (2008) 483–488. https://doi.org/10.1016/j.polymdegradstab.2007.11.009.
[42] C. Lin, D.D.L. Chung, Effect of carbon black structure on the effectiveness of carbon black thermal interface pastes, Carbon. 45 (2007) 2922–2931. https://doi.org/10.1016/j.carbon.2007.10.006.
[43] I. Farahbakhsh, Z. Ahmadi, M. Shahedi Asl, Densification, microstructure and mechanical properties of hot pressed ZrB2–SiC ceramic doped with nano-sized carbon black, Ceram. Int. 43 (2017) 8411–8417. https://doi.org/10.1016/j.ceramint.2017.03.188.
[44] G.R Anstis, P. Chantikul, B.R. Lawn, D.B. Marshall, A critical evaluation of indentation techniques for measuring fracture toughness: I, direct crack measurements, J. Am. Ceram. Soc. 64 (1981) 533–538 https://doi.org/10.1111/j.1151-2916.1981.tb10320.x.
[45] L.F. Nielsen, Elasticity and damping of porous materials and impregnated materials, J. Am. Ceram. Soc. 67 (1984) 93–98. https://doi.org/10.1111/j.1151-2916.1984.tb09622.x.
[46] V.I. Ivashchenko, P.E.A. Turchi, V.I. Shevchenko, N.R. Mediukh, L. Gorb, J. Leszczynski, Phase diagram, electronic, mechanical and thermodynamic properties of TiB2–ZrB2 solid solutions: A first-principles study, Mater. Chem. Phys. 263 (2021) 124340. https://doi.org/10.1016/j.matchemphys.2021.124340.
[47] I. Farahbakhsh, Z. Ahmadi, M. Shahedi Asl, Densification, microstructure and mechanical properties of hot pressed ZrB2–SiC ceramic doped with nano-sized carbon black, Ceram. Int. 43 (2017) 8411–8417. https://doi.org/10.1016/j.ceramint.2017.03.188.
[48] S. Zhou, Z. Wang, X. Sun, J. Han, Microstructure, mechanical properties and thermal shock resistance of zirconium diboride containing silicon carbide ceramic toughened by carbon black, Mater. Chem. Phys. 122 (2010) 470–473. https://doi.org/10.1016/j.matchemphys.2010.03.028.